Compression Failure Mechanisms in Unidirectional Composites

P M Jelf and N A Fleck

Cambridge University Engineering Department
Trumpington Street
Cambridge CB2 1PZ
UK

Abstract

The compressive failure of unidirectional fibre composites has been examined. Four mechanisms of failure have been identified : fibre failure, elastic microbuckling, matrix failure, and plastic microbuckling. Theoretical models to predict the onset of these mechanisms have been reviewed and validated using both model materials and data from the literature. Plastic microbuckling is identified as the dominant compressive failure mechanism in polymeric matrix composites ; for this failure mode compressive strength is dictated by the shear yield strength of the matrix and the misalignment of the fibres. Preliminary work has been undertaken to compare predicted and measured distributions of fibre waviness in a carbon AS4/PEEK composite. Weibull statistics have been used successfully to characterise the compressive failure of unidirectional AS4/PEEK composite.

1. Introduction

There is no consensus in the literature concerning the mechanisms of compressive failure of unidirectional composites. Initial work suggested that compression failure is by a fibre buckling process involving linear elastic matrix deformation [1,2]. An alternative view is that fibre microbuckling is associated with a non-linear response of the matrix, see for example [3-5]. There is also experimental evidence that fibre crushing and matrix failure can result in compressive failure. All these failure mechanisms are depicted in Figure 1.

In the present paper composite materials are developed in order to demonstrate the competition between these mechanisms. Use of model materials enables easy control of composite properties. Failure mechanism diagrams are presented which display the operative failure modes as a function of material properties. Most modern commercial fibre composites fail by plastic microbuckling. As a case study we report the compressive strength for AS4 carbon fibre/PEEK unidirectional specimens and show that the strength follows a Weibull distribution. A size effect on unnotched and notched strength is noted, and is in agreement with the predictions of the Weibull theory.

2. Theory

We summarise in turn current theories of compressive failure due to elastic microbuckling, fibre crushing, matrix failure, and plastic microbuckling.

2.1 Elastic microbuckling

Most attempts to model fibre buckling failure assume elastic bending of the fibres and elastic shear of the matrix, and are modified forms of the theory presented by Rosen [2]. Using a two dimensional model, Rosen assumed that there are two possible buckling modes : a mode where the matrix undergoes extensional straining transverse to the fibre direction, and a mode where the matrix shears parallel to the fibres, see Fig. 1b. In composites containing a significant volume fraction of fibres ($V_f > 0.3$), the shear mode gives lower failure loads. Rosen assumed that the fibres are initially perfectly aligned and calculated the buckling load at which the fibres deflect into a sinusoidal shape. Rosen found that the composite compressive strength σ_c is,

$$\sigma_c = \frac{G_m}{1-V_f} + \frac{\pi^2 E_f}{3}\left(\frac{d}{\lambda}\right)^2 V_f \qquad (1)$$

where V_f and E_f are the fibre volume fraction and modulus respectively, G_m is the matrix shear modulus, d the fibre diameter, and λ is the buckling wavelength. The observed strength of composites reported in the literature is at least a factor of 2 lower than that predicted by equation (1).

2.2 Fibre Crushing

Fibre crushing occurs when the axial strain in the composite attains a critical value equal to the crushing strain of the fibres, ε_{fc}. Fibre failure can occur by longitudinal splitting (of silica glass for example), plastic yielding (metallic fibres), kinking within the fibres (eg.woods) or by plastic buckling of the microstructural units within each fibre (Kevlar).

Fibre collapse is sketched in Fig. 1c.

2.3 Matrix failure

Matrix failure occurs when the axial strain in the composite reaches a critical value equal to the failure strain of the matrix ε_{fm}. The mechanism of failure is brittle crack propagation in the matrix material (see Fig. 1d). This failure criterion predicts a failure stress σ_c of

$$\sigma_c = \sigma_m \left(\left[\frac{V_f E_f}{E_m} \right] + \left[1 - V_f \right] \right) \qquad (2)$$

where σ_m is the failure strength of the matrix alone, E_f and E_m are the fibre and matrix Young's moduli respectively, and V_f is the volume fraction of fibres. It is thought that this mechanism operates in ceramic matrix composites such as silicon fibres in a pyroceramic matrix at quasi-static strain rates [7].

2.4 Plastic microbuckling

Argon[8] and also Budiansky [9] identified the shear yield stress k of the matrix and the initial fibre misalignment angle $\bar{\phi}$ of the fibres as the main factors controlling compressive strength. For a rigid-perfectly plastic body Budiansky showed that

$$\sigma = \frac{k^*}{\bar{\phi} + \phi} \qquad (3)$$

where $\bar{\phi}$ is the assumed fibre misalignment angle in the kink band, ϕ is the additonal fibre rotation in the kink band under a remote stress σ, and

$$k^* = k \left(1 + \left(\frac{\sigma_{Ty}}{k} \right)^2 \tan^2 \beta \right)^{\frac{1}{2}} \qquad (4)$$

Here k and σ_{Ty} are the in-plane shear and transverse yield strengths of the composite respectively. The band orientation β and fibre rotations $\bar{\phi}$ and ϕ are shown in Figure 2a. The critical stress $\sigma=\sigma_c$ is achieved at $\phi = 0$ in equation (3). In the case $\beta=0$ equations (3) and (4) simplify to Argon's result [8]

$$\sigma_c = \frac{k}{\bar{\phi}} \qquad (5)$$

Argon[8], Budiansky [9], and Fleck and Budiansky [10] neglect fibre bending in their analysis of microbuckling : they treat the problem as one of fibre kinking. Plastic microbuckling is thought to occur in a region of relatively misaligned fibres (see Figure 2b). Fibre breakage sets the width w of the microbuckled band. Budiansky[9] has predicted w using an elastic bending analysis as,

$$\frac{w}{d} = \frac{\pi}{4} \left(\frac{V_f E_f}{2k} \right)^{\frac{1}{3}} \qquad (6)$$

where d is the fibre diameter.

3. Tests on model materials

Model materials were used to demonstrate the four failure modes : elastic microbuckling, fibre crushing, matrix failure, and plastic microbuckling. Glass fibres in a silicone elastomer matrix, and wheat flour fibres (spaghetti) in a silicone elastomer matrix failed by elastic microbuckling. Pine wood fibres in a ductile dental modelling wax underwent fibre collapse. Composites consisting of wheat flour fibres in a brittle wax, and glass fibres in a Plaster of Paris matrix suffered matrix failure. Plastic microbuckling occurred in composites consisting of a ductile wax matrix and fibres of either glass, copper, or wheat flour. In addition metal matrix composite (glass fibres in a lead-tin solder) and AS4 carbon fibres in PEEK matrix failed by plastic microbuckling.

The model materials were fabricated as follows. Fibres were held in a regular hexagonal array of centre-centre spacing 3mm by a wire mesh at each end of a mould. The mould was subsequently filled with the appropriate matrix material. This process produced composite materials with a fibre volume fraction in the range 0.3 to 0.4. Compression tests were performed on rectangular section testpieces (generally width W=45mm and thickness t=8mm and height in the range 60-170mm). The testpieces were compressed between flat plattens at a rate of 0.02mm/sec. Euler macrobuckling was suppressed by using lubricated anti-buckling guides, see Figure 3. During testing the antibuckling guides were loosened at regular intervals to compensate for the specimen thickening under load due to Poisson effects.

Tables 1 to 4 give material properties of the model composites and their constituent materials. The measurement of composite compressive strength is detailed in the sections below. The methods for measuring fibre and matrix properties are given in Appendix I.

The volume fraction of fibres V_f in the composite was measured by transverse sectioning each composite and calculating the ratio of fibre area to total section area. Results are shown in Table 4. The shear modulus G and shear strength k of the glass/silicone elastomer composite was determined by applying simple shear to a plate specimen of dimensions w=45mm, t=8mm, and h=170mm. The axial modulus E and in-plane shear modulus G of the other model composites were deduced from the constituent fibre and matrix properties using the inverse rule of mixtures approximation. Values are summarised in Table 4.

3.1 Elastic microbuckling

Elastic fibre microbuckling requires the matrix material to behave in a linear elastic fashion up to high strains. The majority of commercially available composite materials do not satisfy this requirement. In order to test Rosen's elastic microbuckling theory we fabricated a model material where the matrix behaved in a linear elastic manner. Composite specimens were made using Dow-Corning Sylgard 184 silicon elastomer matrix. The properties of the matrix were examined by axially compressing cylindrical specimens of elastomer. The specimens of height 10mm, diameter 15mm were lubricated top and bottom in order to minimise frictional effects due to Poisson expansion. Little barrelling was noted during testing. The true stress versus logarithmic strain

response was linear over the measured strain range of 0 to 0.7. Two types of fibre were used in the model composites ; glass rods or wheat flour fibres (spaghetti) both of diameter d=2mm. These fibres were chosen because of their greatly differing elastic properties. For glass E=69 GPa whilst for spaghetti E=2.9 GPa.

Compressive failure of these model composites was by in-plane elastic microbuckling with the Rosen wavelength λ equal to twice the specimen height. A single plane of fibre breakage was observed, which propagated across the specimen at an angle β=0° to the horizontal. Debonding over a total length of approximately 6 fibre diameters accompanied fibre fracture. The debond zone was symmetrical to the fracture plane of the fibres. The observed failure loads are much less than those predicted by classical Euler buckling. The effect of buckle wavelength λ=2h was determined by varying the specimen height. Good agreement is noted between the prediction (1) and the observed strengths of spaghetti/elastomer specimens ; see Figure 4. As the specimen length increases the contribution of fibre bending to the composite strength decreases and the first term in equation (1) becomes dominant. Glass/elastomer specimens (λ/d=170) fail at a stress σ_c=1.54 MPa which is almost equal to the composite shear stiffness (measured explicitly in a separate test) of G_{comp} = 1.56 MPa.

We conclude that Rosen's equation (1) is accurate when the matrix behaves in a linear elastic fashion. Most previous attempts to fit experimental data with this model have involved empirical correlation factors (e.g.Lager and June [11]). Most load bearing composites contain matrices which do not deform in a linear elastic manner.

3.2 Fibre Crushing

The model material consisted of a 30% volume fraction of slender wooden rods (diameter d=2mm) in a ductile wax matrix. The wooden fibres were commercial cocktail sticks made from pine. The wax was Pinnacle dental modelling wax. The uniaxial compressive stress versus strain response of the wax is shown in Figure 5. The wax behaves almost in an elastic-perfectly plastic manner. The measured strength of the wooden rods was obtained through use of a Celanese compression rig - this rig is documented in [12]. The salient properties of the wax and wood are summarised in Tables 1 and 2 respectively. Compression tests were performed on composite specimens of length 54mm, width 48mm, and thickness 10mm. Direct end loading was applied via the platens of a screw driven test machine. The composite failed by crushing of the wood, at an average stress of σ_c=11.1 MPa for 3 specimens. The rule-of-mixtures formula,

$$\sigma_c = V_f \sigma_{fc} + (1 - V_f)\, \sigma_{my} \qquad (7)$$

suggests a compressive strength of 11.2 MPa, where σ_{fc} is the fibre crushing strength and σ_{my} is the matrix yield strength. We conclude that the rule of mixtures provides an adequate approximation for the composite strength.

3.3 Matrix failure

Two model materials were developed where the composite failure was governed by brittle failure of the matrix : spaghetti fibres in a brittle paraffin wax matrix, and slender glass rods in calcium sulphate hemihydrate ($CaSO_4.^1/2H_2O$ - Plaster of Paris) matrix. In both cases the fibre diameter was 2mm. The uniaxial compressive response of the paraffin wax and Plaster of Paris is shown in Fig.5. Properties of these fibres and matrices are given in Tables 1 and 2. Compression tests were performed on rectangular section testpieces (width 30-50mm, thickness=8mm, height 80-140mm) subjected to direct end-loading. Euler buckling was inhibited by anti-buckling guides.

Both composite materials exhibited matrix failure. The average compressive failure strain of the paraffin wax alone was 1.28%, whilst the spaghetti/paraffin wax composite failed at an average axial compressive strain of 1.23%. The failure strain of $CaSO_4.^1/2H_2O$ was 0.234%, and the glass/ $CaSO_4.^1/2H_2O$ composite failure strain was 0.226%.

We conclude that the composite fails when the compressive strain equals the failure strain of the matrix.

3.4 Plastic microbuckling

Composites were manufactured from a ductile wax matrix in order to examine fibre buckling failure in which matrix plasticity was assured. Three types of fibre were used : glass rods, annealed copper wire, and spaghetti. Plastic microbuckling was observed in all three systems and composite compressive strengths are given in Table 3. During fabrication the low modulus spaghetti fibres became wavy due to the thermal contraction of the cooling matrix material. The copper wire possessed an average residual curvature of radius 2.2m from their initially coiled state. The glass rods were manufactured with negligable curvature. Further fibre misalignment was inevitably introduced during manufacture of the model composites. Measurements of the fibre misalignment induced by the above factors are given in Table 3 ; fibre misalignment angle was measured from micrographs of the surface of specimens, using a protractor. Equation (5) was used to infer fibre misalignment angles $\bar{\phi}$ from the measured strengths. These values are included in Table 3. Excellent agreement is noted between the measured and inferred angles. We conclude that equation (5) gives accurate predictions of the compression strength from measured values of k and $\bar{\phi}$.

Now consider a model metal matrix composite (MMC) manufactured using glass rods (diameter d=2mm) in a matrix of plumber's solder (an alloy of 60% lead, 40% tin). Fibre and matrix properties are given in Tables 1 and 2. Compressive tests were undertaken using rectangular section specimens (width w=30mm, thickness t=8mm, height h=140mm). The average compressive failure stress for 5 specimens was 252 MPa. The fibre misalignment angle $\bar{\phi}$=4.1° inferred from the measured strength using equation (5) is in good agreement with observed fibre misalignments of $\bar{\phi}$=2-4°. The material failed in a band inclined at an angle of approximately β=30°. Equation (6) predicts a microbuckle band width of 12.9mm for this material. Fragments ejected from the central failed region of the MMC specimens were typically 12mm in height. We conclude that this metal matrix composite fails by plastic microbuckling.

For all the model composites tested, fibre/matrix debonding occurred only to within 4 fibre

diameters of the fibre breaks and was a consequence of fibre fracture. We conclude that debonding does not control the buckling strength.

4. Analysis of plastic microbuckling data from literature

Equation (5) suggests a linear relation between the compressive strength of a unidirectional composite σ_c, and the in-plane shear yield stress, k. Experimental data for unidirectional composites (mainly with a polymeric matrix) are taken from the literature in addition to the current study, and are displayed as a log-log plot of σ_c versus k, see Fig.6. Values of k are defined as the in-plane shear stress at an in-plane shear strain γ=1%. It is noted that the data for σ_c and for k span two orders of magnitude. We find that σ_c is linear in k, and that the constant of proportionality suggests $\bar{\phi}$=3.0° from equation (5). The predicted angle of $\bar{\phi}$ is 3.7° via equation (6), where we assume a band angle β=20°, and $\sigma_{Ty}/k = 2$. These predicted values of $\bar{\phi}$ are physically reasonable.

The predicted kink width w from equation (6) is compared in Fig.7 with measured values of kink width from the current study and from the literature. A regression of the data shows that the kink width w satisfies the relation,

$$\frac{w}{d} = 0.68 \left(\frac{V_f E_f}{k}\right)^{0.37} \qquad (8)$$

The theoretical prediction of Budiansky[9], equation (6) is in excellent agreement with this empirical expression for the measured kink width. We note that kink width scales linearly with fibre diameter. The use of large diameter fibres (d=2mm) in the model materials enables easy and accurate observation of the kink width.

5. Case study : compressive failure of carbon fibre/PEEK

Modern polymeric matrix composite systems usually fail by plastic microbuckling. As a case study we have measured the compressive strength of an AS4 carbon fibre/PEEK composite, APC-2, produced by ICI Fiberite. Attention was focussed on the variability of strength.

Compressive tests were performed on 25 specimens made from a 16 ply unidirectional lay-up. The specimen geometry is shown in Fig.8, and tests were performed using a Celanese test rig [12]. The measured distribution of strength is shown in Fig.9a ; the strength varies from 800 to 1350 MPa, with a mean value of 1109 MPa.

We interpret the spread in strength as a reflection of the variability in misalignment angle $\bar{\phi}$ from specimen to specimen. Fig.9b shows the fibre misalignment angle $\bar{\phi}$ inferred from equation (5), where we have used the compressive strength data of Fig.9a, and assumed k=40 MPa.The inferred values of $\bar{\phi}$ range from 1.7° to 2.8°.

Yurgatis[13] has measured directly the spread in fibre misalignment in AS4/PEEK material by a sectioning technique. His results are included in Fig.9b, and show that $\bar{\phi}$ lies in the range 0-4°.

The difference between measured and inferred $\bar{\phi}$ distributions is consistent with the deduction that infrequent highly misaligned fibres do not result in failure; a concentration of interacting misaligned fibres is necessary. There is not a one-to-one correspondence between measured and predicted misalignment angles. Further studies are necessary in order to consider the mechanics of microbuckle initiation and to establish the functional dependence of compressive strength upon the distribution of misalignment angle.

The spread in compressive strength of the AS4/PEEK material may be characterised in terms of the Weibull theory of strength. The Weibull theory is a weakest link theory of fracture, and has been used successfully in characterising the probability of tensile failure in ceramics.

6. Weibull analysis

The Weibull theory predicts that the probability of survival P_s of a material of volume V under uniaxial stress σ is given by,

$$P_s(V) = \exp\left[-\int_o^V \left(\frac{\sigma - \sigma_u}{\sigma_0}\right)^m \frac{dV}{V_0}\right] \qquad (9)$$

where σ_u is a minimum cut-off strength, σ_0 is a normalising strength, V_0 is a reference volume and the Weibull index m gives a measure of the spread in strength.

A best fit of the compression strength of the 25 specimens of AS4/PEEK is shown in Figure 10. We find that m=6.1, σ_u=350 MPa, and σ_0=805 MPa for $V=V_o=240mm^3$. The low value of m is comparable to that for ceramic materials.

The Weibull theory predicts that the strength is dependent upon the stressed volume, and that the mean strength of a specimen is size dependant. In order to test this,we performed compression tests on two geometrically similar specimens, using the Celanese test rig.The specimens were made from 3mm thick $(0/90)_{4S}$ lay-up AS4/PEEK material, and contained a central hole of diameter D=0.25 times the specimen width W. The first set of 5 specimens were of gauge length l_1=12mm, and width W_1=4mm, while the second set of 4 specimens were of gauge length l_2=12mm and width W_2=10mm. The average failure strength of the first set of specimens (based on gross section) was σ_1=501 MPa, and the average failure strength of the second set was σ_2=452 MPa. The Weibull prediction,

$$\frac{\sigma_2 - \sigma_u}{\sigma_1 - \sigma_u} = \left(\frac{W_1}{W_2}\right)^{1/m} \qquad (10)$$

suggests m=7.0. This value of m is in good agreement with the value m=6.1 deduced from the spread in unidirectional strength of unnotched specimens of constant size. Here, we are not using Weibull statistics to predict notched strength from unnotched strength; rather we are showing that the notch size effect may be interpreted in terms of the Weibull theory.

7. Failure Mechanism Diagrams

Failure mechanisms exhibited by unidirectional fibre composites may be summarised in a failure diagram with axes $k/\bar{\phi}$ and $G_m/(1-V_f)$. Failure is shown by four distinct mechanisms:

a) Elastic microbuckling, predicted by the Rosen equation (1).

b) Plastic microbuckling, predicted by the Argon equation (5).

c) Matrix failure at a strength given by equation (2).

d) Fibre crushing at a strength predicted by equation (7).

Figures 11a-d show a failure map for 4 model materials. Each map is divided into three regions : elastic microbuckling, plastic microbuckling, and one of either fibre crushing or matrix failure depending upon which of these two mechanisms gives the lower failure stress.
Contours of predicted strength are given by equations (1) and (5). A point is plotted on each map at co-ordinates $(G_m/(1-V_f), k/\bar{\phi})$ and its location indicates both the composite's expected failure mode and strength. The glass/elastomer composite failed by elastic microbuckling, see Fig.11a. Copper wires in ductile wax fail by plastic microbuckling, Fig.11b, whilst spaghetti in brittle paraffin wax fail by matrix fracture, Fig.11c. Wood fibres in ductile wax experiences fibre crushing, as shown in Fig.11d. The predicted failure modes and strengths are in good agreement with the experimental data in all four cases.

A failure map for carbon fibre - PEEK and carbon fibre - epoxy composites is shown in Fig. 11e, where we have assumed $\bar{\phi} = 3°$. This value for $\bar{\phi}$ is similar to that observed by Yurgatis [13] for AS4/PEEK, and that inferred from Fig. 6 for several composites. We note from Fig. 11e that failure is always by plastic microbuckling.

8. Concluding Remarks

We conclude that plastic microbuckling is the mechanism by which most modern load-bearing fibre composites fail. The Argon/Budiansky model [8,9] is shown to be accurate in predicting failure by this mechanism. The model uses the parameters of matrix shear yield strength and an average initial fibre misalignment angle. In brittle matrix composites, the matrix non-linearity may be due to distributed microcracking rather that plasticity. Recently, Budiansky and Fleck [24] have modelled microbuckling of fibre composites by assuming that the matrix behaves as a non-linear deformation theory solid. The non-linearity can either be due to microcracking or to plasticity.

Acknowledgements

This work was carried out with the financial support of the Procurement Executive of the Ministry of Defence and the Science and Engineering Research Council (SERC). The authors are grateful for helpful discussions with Dr P T Curtis, Dr Y Rajapske, Prof. M F Ashby, and Prof. B Budiansky.

References

1. Dow, N.F. and Gruntfest, I.J., 1960, "Determination of Most-Needed, Potentially Possible Improvements in Materials for Ballistic and Space Vehicles", General Electric, Air Force Contract AF04(647)-269

2. Rosen, B.W., 1964, "Mechanics of Composite Strengthening. Fiber Composite Materials", *American Society of Metals*, pp. 37-45

3. Fried, N., 1963, "The Compressive Strength of Parallel Filament Reinforced Plastics - The Role of the Resin.", *Proceedings of the 18th Annual Meeting of the Reinforced Plastics Division*, Society of Plastic Industry

4. Chaplin, C.R., 1977, "Compressive Fracture in Unidirectional Glass-Reinforced Plastics", *Journal of Materials Science* 12, pp. 347-352

5. Soutis, C., and Fleck, N.A., 1990, "Static Compression Failure of Carbon Fibre T800/924C Composite Plate with a Single Hole.", *Journal of Composite Materials* 24, pp.536-558

6. Hahn, H.T., 1986, "Compression Failure Mechanisms of Composite Structures", NASA CR-3988

7. Lankford, J.,1989, "Dynamic compressive fracture in fiber reinforced ceramic matrix composites", *Mat. Sci. and Engng.* , A107, pp 261-268

8. Argon, A.S., 1972, "Fracture of Composites", *Treatise of Material Science And Technology* , Vol. 1, Academic Press, New York

9. Budiansky, B., 1983, "Micromechanics", *Computers and Structures* , 16(1-4), pp.3-12

10. Fleck, N.A., and Budiansky, B., 1990, "Compressive Failure of Fibre Composites due to Microbuckling", in 'Inelastic Deformation of Composite Materials', ed. G.J. Dvorak, Springer-Verlag, pp. 235-274

11. Lager, J.B., and June, R.R., 1969, "Compressive Strength of Boron/Epoxy Composites" *Journal of Composite Materials* , 3(1), pp. 48-56

12. Curtis, P.T., 1985, "CRAG Test Methods for the Measurement of the Engineering Properties of Fibre Reinforced Plastics", RAE Technical Report TR-85099

13. Yurgatis, S.W., 1987, "Measurement of Small Angle Fiber Misalignments in Continuous Fiber Composites", *Composites Science and Technology* , Vol. 30, pp. 279-293

14. Soutis, C., 1989, "Compressive Failure of Notched Carbon Fibre-Epoxy Panels", Ph.D. Thesis, Cambridge University Engineering Department, England

15. Curtis, P.T., 1986, "An investigation of the mechanical properties of improved carbon fibre composite materials", RAE Technical Report TR-86021

16. Johnston, N.J., and Hergenrother, P.M., 1987, "High Performance Thermoplastics : A Review of Neat Resin and Composite Properties", *Proceedings of 32nd International SAMPE Symposium* , April 6-9 1987, pp.1400-1412

17. Fried, N., and Kaminetsky, J., 1964, "Influence of Material Variables on the Compressive Properties of Parallel Filament Reinforced Plastics", *19th Conference of the Society of Plastics Industry - Reinforced Plastics Division* , February 1964, Section 9A, pp. 1-10

18. Eilfort,S.K., and Petker, R., 1964, "Resin Systems for Filament Wound High External Load Bearing Structures", *19th Conference of the Society of Plastics Industry - Reinforced Plastics Division* , February 1964, Section 14B

19. Piggott, M.R., Harris, B., 1980, "Compression Strength of Carbon, Glass, and Kevlar 49 Fibre Reinforced Polyester Resins", *Journal of Materials Science* 15(1980), pp. 2523-2538

20. Wronski, A.S., Parry, T.V., 1982, "Compressive failure and kinking in uniaxially aligned glass-resin composite under superposed hydrostatic pressure", *Journal of Materials Science* 17(1982), pp. 3656-3662

21. Piggott, M.R., Wilde, P., 1980, "Compressive strength of aligned steel reinforced epoxy resin", *Journal of Materials Science* 15(1980), pp. 2811-2815

22. El-Magd, E., Dackweiter, G., 1990, "Deformation mode of fibre metal composites under impact compression", *Proceedings of 4th ECCM* , Sept. 25-28 1990, Stuttgart FRG, 369-374

23. US Polymeric data sheet, 1988, US polymeric, BP Chemicals, Advanced Materials Division, Santa Anna, California, USA

24. Budiansky B. and Fleck N.A., 1992. "Compressive Failure of Fibre Composites",to appear in the Journal of Mechanics and Physics of Solids.

25. Jelf, P.M., and Fleck, N.A., 1992, "Failure of Composite Tubes under Combined Compression and Torsion Loading", *submitted to J. Materials Science*

26. Guynn E.G, et al., 1989, "A Comparison of Experimental Observations and Numerical Predictions for the Initiation of Fiber Microbuckling in Notched Composite Laminates", presented at 3rd ASTM Symposium on Composite Materials,Lake Buena Vista, Florida, Nov.6-9 1989

27. Batdorf, S.B., and Ko, R.W.C., 1987, "Stress-strain Behaviour and Failure of Uniaxial Composites in Combined Shear and Compression,Parts I and II", Internal Report, School of Engineering and Applied Science, University of California, Los Angeles, CA 90024

Appendix I - Experimental Techniques

Tests on Model Fibres

The compressive strength σ_{fc} of the non-brittle fibres (spaghetti, pine wood, and copper) was measured by testing bundles of 4 to 5 fibres in a Celanese test rig (see [12]). Data for the brittle glass fibres was gathered by compressing circular cylinders (diameter d=12mm, height h=8mm) of silica glass between flat platens.

Values of fibre modulus E were obtained from tensile tests on bundles of 4 to 5 fibres using a screw driven test machine, at a nominal strain rate of 4×10^{-4} s^{-1}. Fibre strain was monitored using a clip gauge extensometer. A textbook value of Young's modulus for the silica glass was assumed.

Tests on Model Matrices

Circular cylinders of matrix material (ductile modelling wax, paraffin wax, plaster-of-Paris, silicone elastomer, and plumber's solder) of dimension diameter d=25mm and height h=20mm were compressed between flat platens at a strain rate of 4×10^{-4} s^{-1}. The platens were lubricated to minimise frictional effects and barrelling. The Young's modulus E was calculated from nominal stress and strain. Values of shear yield stress k where inferred from the nominal yield stress σ_y using the Tresca criterion $k=\sigma_y / 2$. In general values of shear modulus G were inferred from the Young's modulus E, assuming isotropic behaviour and a Poisson ratio $\nu = 0.3$.

Table 1 Summary of relevant matrix properties
(*) = brittle failure

	Matrix				
	Dow Corning Sylgard 184 Silicon elastomer	Ductile Modelling Wax	Plumbers Solder	Plaster of Paris	Paraffin Wax
Compressive Modulus E (MPa)	2.8	75	3940	5300	71
Shear modulus G (MPa)	0.94	29	1300	2000	27
Shear or fracture strength k (MPa)	0.98	0.75	18.2	6.2 (*)	0.45 (*)

Table 2 Summary of significant fibre properties

	Fibres			
	Silica Glass	Dry Spaghetti	(Pine) Wood	Cold drawn Copper
Diameter d (mm)	2	2	2	2
Modulus E (GPa)	69	2.9	4.5	120
Compressive Failure Stress (MPa)	420	56	34	500

Table 3 Values of composite strength and fibre misalignment angle for model composites and AS4/PEEK which experience plastic microbuckling

	Model materials				
	Spaghetti/Ductile wax	Glass/Ductile wax	Copper/Ductile wax	Glass/Solder	AS4/PEEK
Composite Compressive Strength (MPa)	21.3	43	22.7	252	1109
Measured $\bar{\phi}$ (°)	2-3	1-2	1-2	2-4	0-4
$\bar{\phi}$ Inferred from equation (4) (°)	2.0	1.0	1.9	4.1	1.7-2.7
Measured β (°)	10	10	10	25	16
Kink width w (mm)	11	40	60	12	0.06

Table 4 Model Composite properties

Composite material	Volume fraction V_f	Compressive strength σ_c (MPa)	Young's modulus E (MPa)	In-plane Shear modulus G (MPa)
Spaghetti/Ductile Wax	0.33	21.3	1010	43
Spaghetti/Paraffin Wax	0.30	11.4	920	39
Wood/Ductile Wax	0.30	11.1	1403	41
Glass/Ductile Wax	0.34	43	23500	45
Copper/Ductile Wax	0.33	22.7	39700	44
Glass/Plaster of Paris	0.32	56.5	25700	2940
Glass/Solder	0.38	252	28900	1910
Glass/Elastomer	0.33	1.54	22800	1.56
Spaghetti/Elastomer	0.31	1.40	900	1.36

List of Figure captions

Figure 1 Failure mechanisms in compression

a) Typical stress-strain response of unidirectional composite. Macroscopic response is elastic-brittle

b) Elastic microbuckling. Two modes are distinguished, shear and extensional

c) Fibre crushing, for example by shear yielding of the fibre or splitting of the fibre

d) Matrix failure

e) Plastic microbuckling

Figure 2a Geometry of an idealised microbuckle

Figure 2b Micrograph of microbuckle in unidirectional carbon/PEEK composite. Specimen was loaded top to bottom of this photograph. Fibre diameter is typically 6-7 μm. The microbuckle band inclination β=16°.

Figure 3 Schematic view of anti-buckling guide used for model material testing.

Figure 4 Elastic buckling of dry wheat flour fibres in silicone elastomer. The Rosen prediction, equation (1) is in good agreement with experimental data. The buckled wavelength equals twice the specimen height.

Figure 5 Compressive stress versus strain response of the model material matrices.

Figure 6 Comparison of microbuckling stress and in-plane shear strength k. The straight line is a best fit to the data and suggests $\bar{\phi}$ = 3° from equation (5).

Figure 7 Comparison of predicted and measured microbuckling. W=microbuckle width,d=fibre diameter, E=composite stiffness, k=matrix shear strength, Vf = volume fraction of fibres. Data regression gives eqn.(8) which agrees well with the prediction (6).

Figure 8 Specimen geometry used in the Celanese compression test.

Figure 9a) Distribution of AS4/PEEK compressive strength. Sample size = 25 specimens.

b) Comparison of measured fibre misalignment angle $\bar{\phi}$ in unidirectional AS4/PEEK taken from Yurgatis [17], and $\bar{\phi}$ inferred from compressive strength data in present study and equation (5). The total area under each curve equals unity.

Figure 10 Weibull analysis of unidirectional AS4/PEEK compressive strength results from present study.

Figure 11 Compression Failure maps

a) Glass/Elastomer composite. The $\left(\frac{G_m}{1 - V_f}, \frac{k}{\bar{\phi}}\right)$ value of the glass/elastomer system is shown by the symbol ● ; $\bar{\phi} = 2°$ assumed. The measured strength $\sigma_c = 1.54$ MPa agreed with the elastic microbuckling stress $\sigma_c = G_m / (1 - V_f) = 1.56$ MPa.

b) Copper/ductile wax composite. $\bar{\phi}$ assumed to be 2°. The measured strength of this composite is 22.7 MPa.

c) Spaghetti/paraffin wax composite. $\bar{\phi}$ assumed to be 2°. The measured strength of this composite is 11.9 MPa.

d) Wood/ductile wax composite. $\bar{\phi}$ assumed to be 2°. The measured strength of this composite is 11.1 MPa.

e) Various carbon fibre composite systems. Predicted strengths are plotted assuming $\bar{\phi} = 3°$.

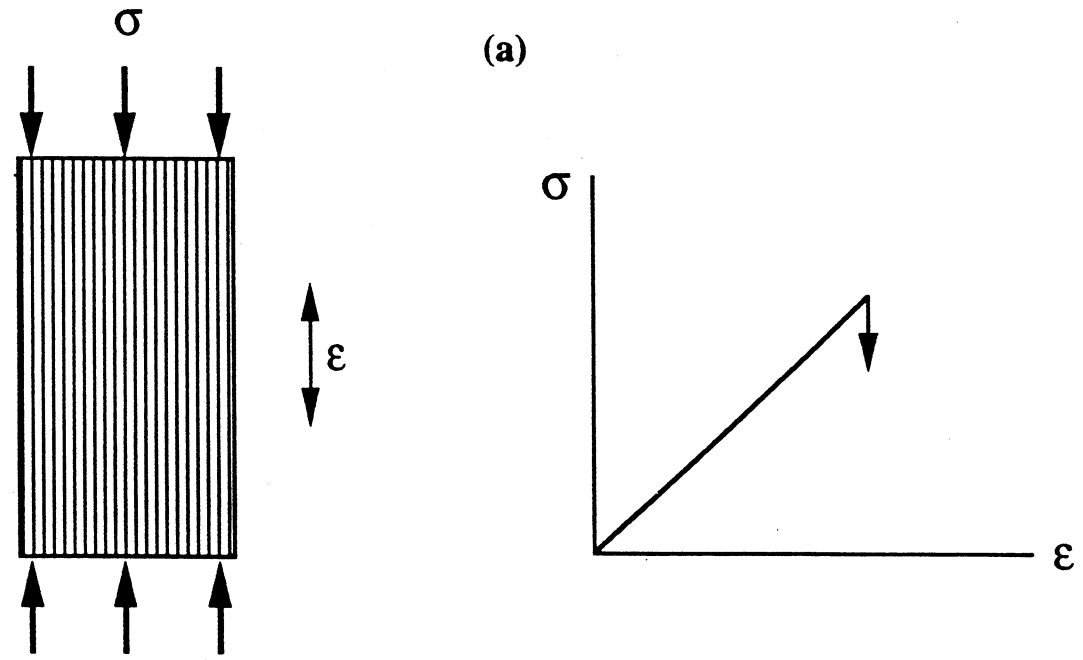
σ
(a)
ε
σ
ε

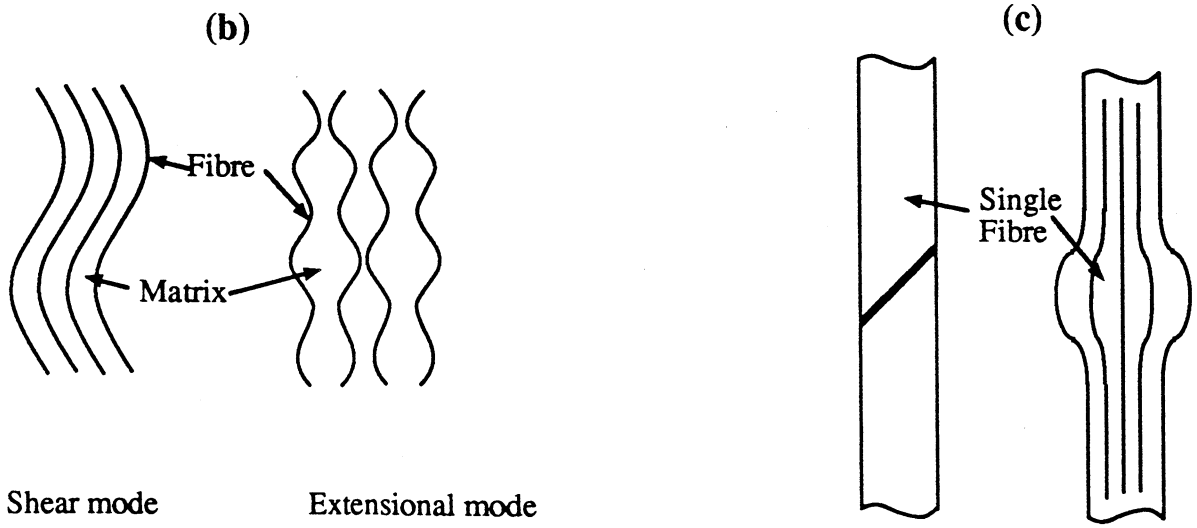
(b)
Fibre
Matrix
Shear mode
Extensional mode
(c)
Single
Fibre

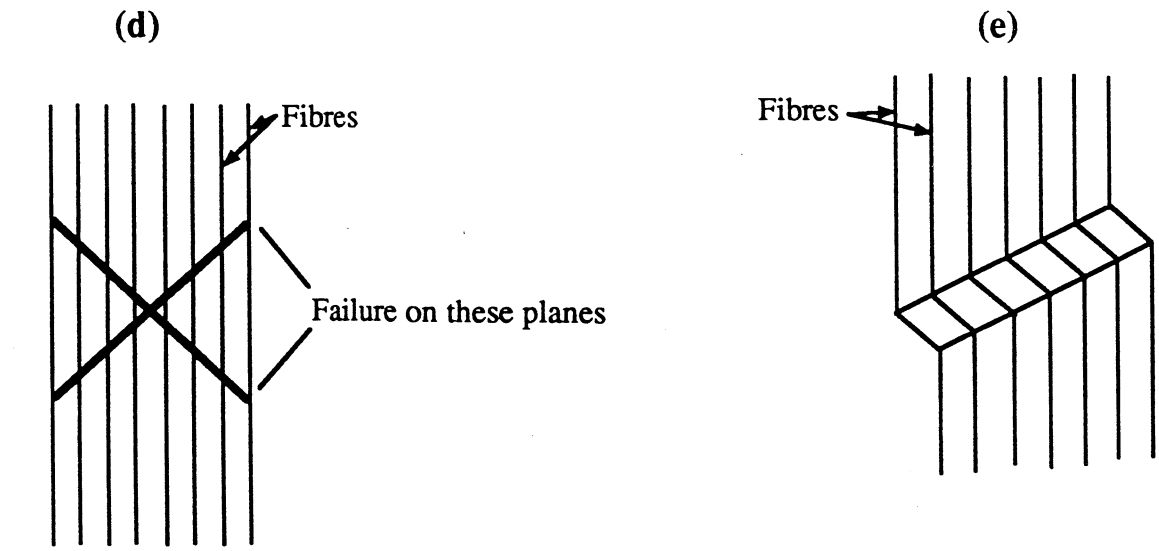
(d)
Fibres
Failure on these planes
(e)
Fibres

Figure 1 (a) - (e)

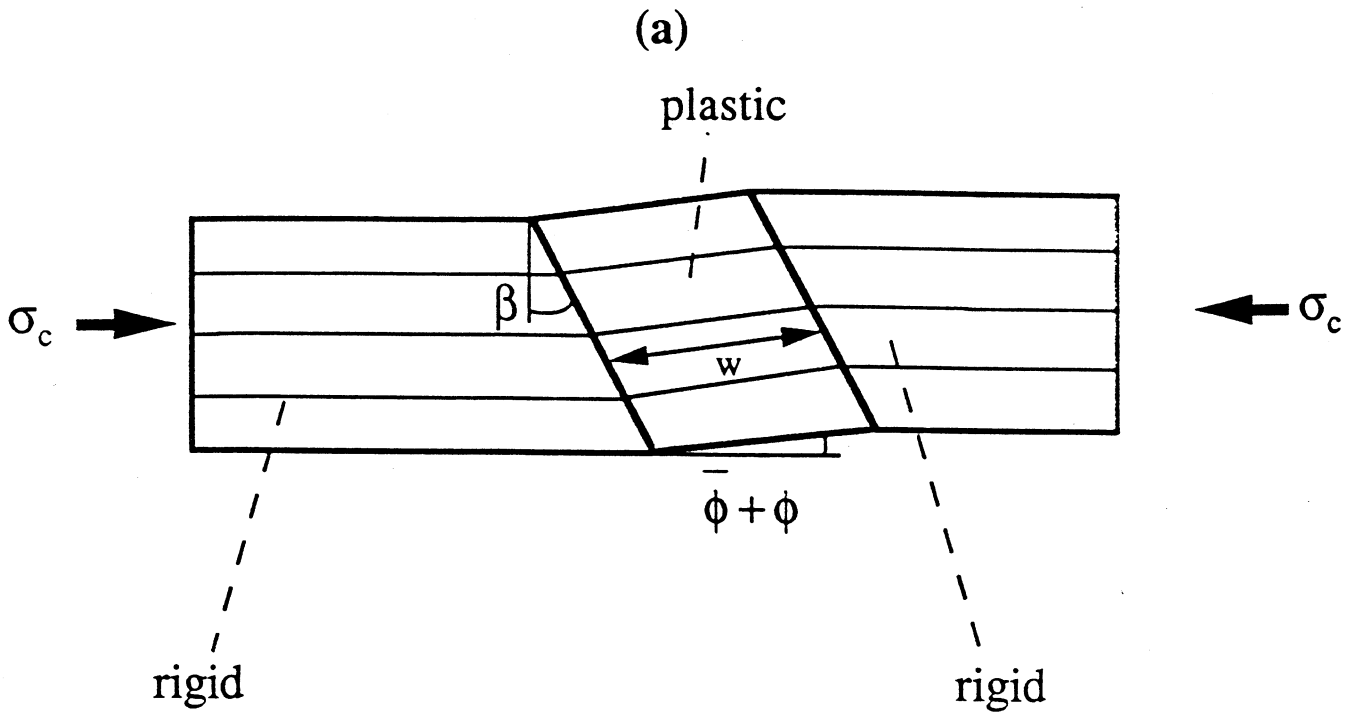

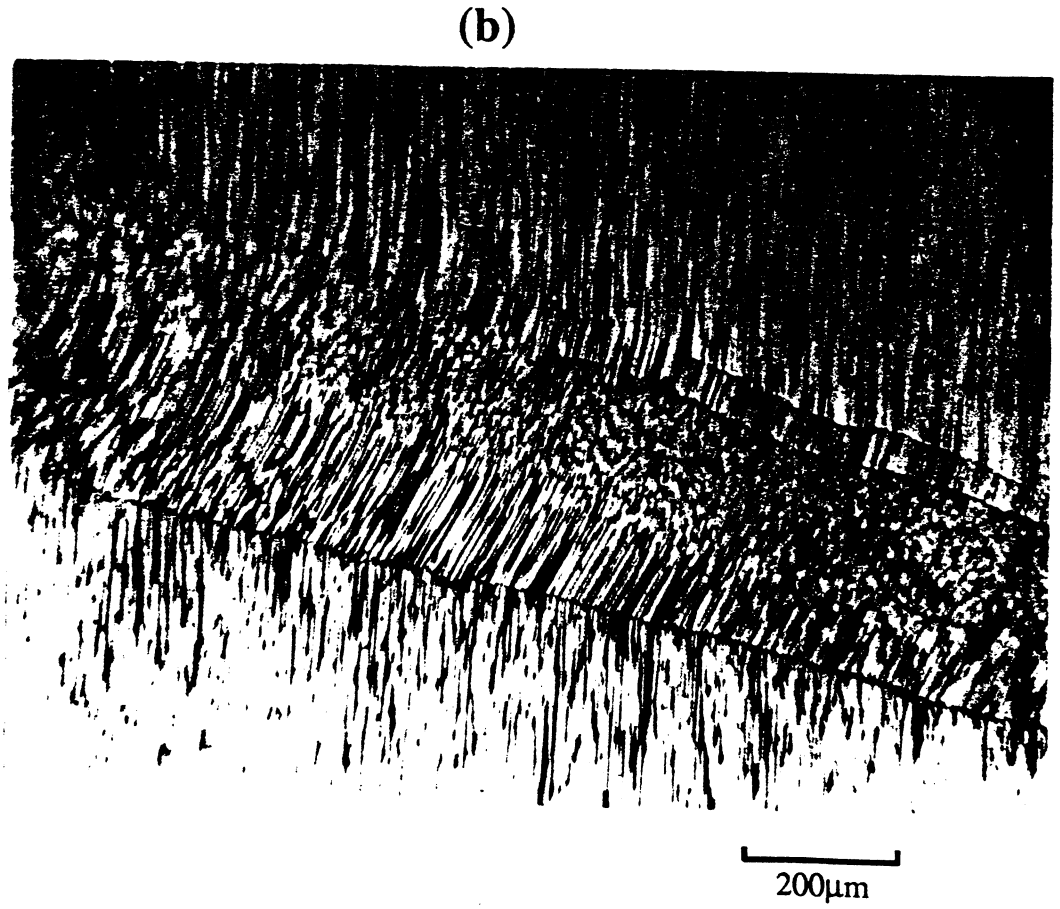

Figure 2 (a) - (b)

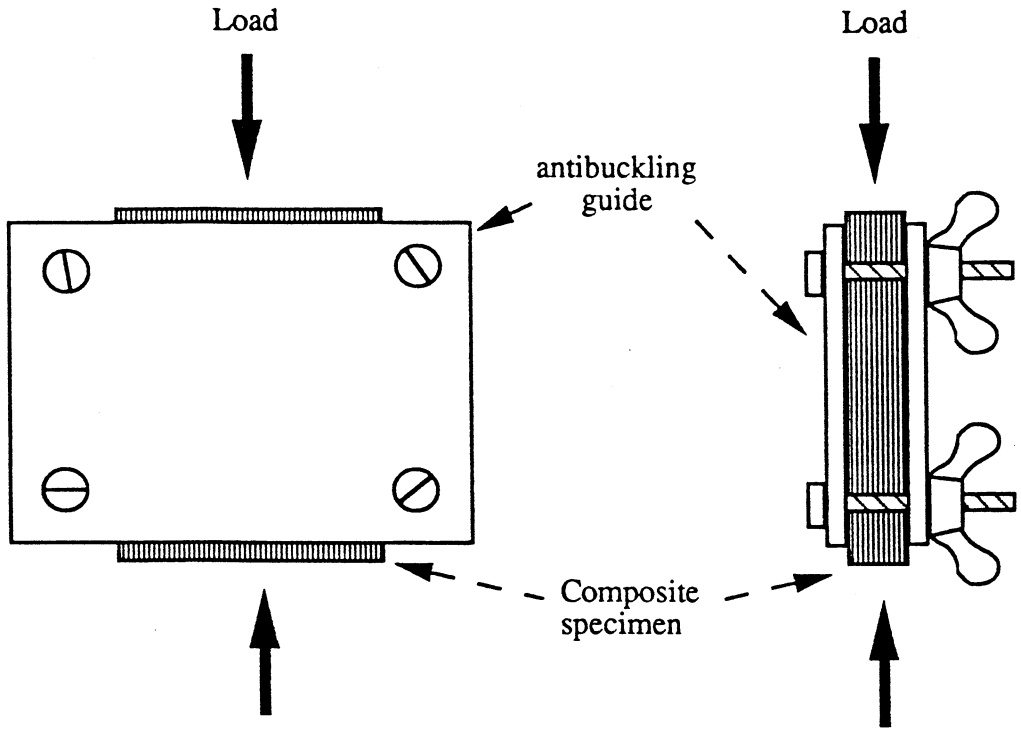

Figure 3

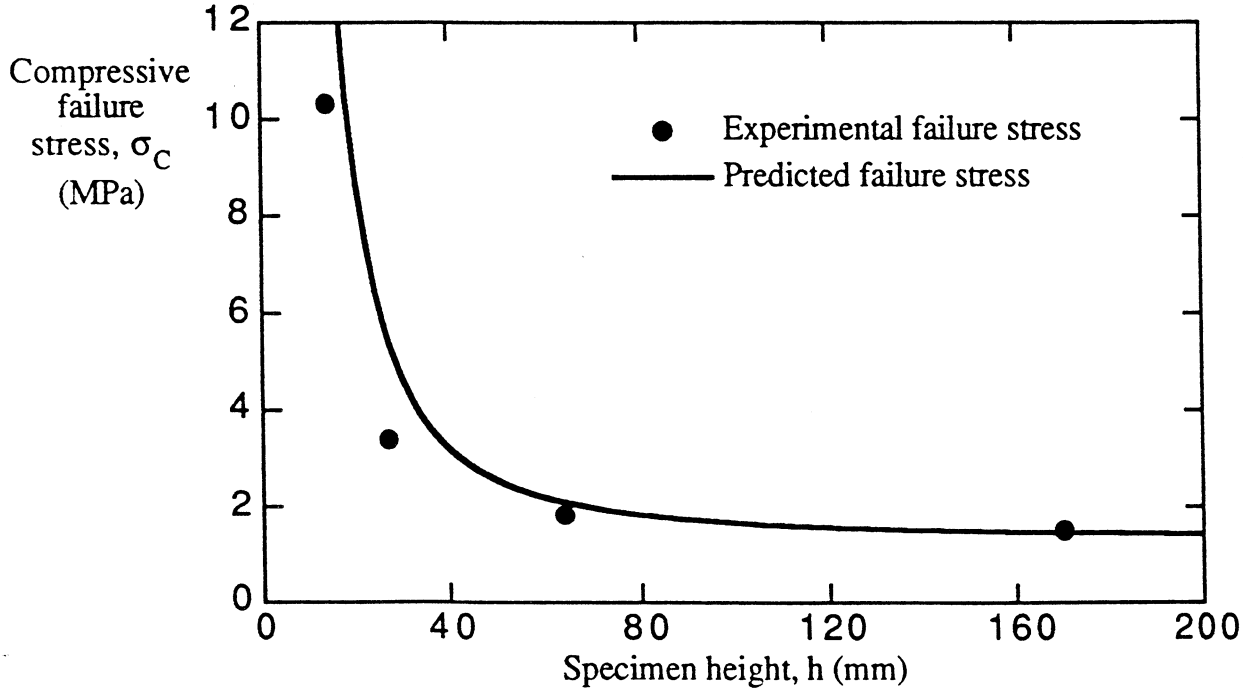

Figure 4